

Get a Grip: Reconstructing Hand-Object Stable Grasps in Egocentric Videos

Zhifan Zhu

Dima Damen

School of Computer Science, University of Bristol, UK

<https://zhifanzhu.github.io/getagrip>

Abstract. We propose the task of Hand-Object Stable Grasp Reconstruction (HO-SGR), the reconstruction of frames during which the hand is stably holding the object. We first develop the stable grasp definition based on the intuition that the in-contact area between the hand and object should remain stable. By analysing the 3D ARCTIC dataset, we identify stable grasp durations and showcase that objects in stable grasps move within a single degree of freedom (1-DoF). We thereby propose a method to jointly optimise all frames within a stable grasp, minimising object motions to a latent 1-DoF. Finally, we extend the knowledge to in-the-wild videos by labelling 2.4K clips of stable grasps. Our proposed EPIC-Grasps dataset includes 390 object instances of 9 categories, featuring stable grasps from videos of daily interactions in 141 environments. Without 3D ground truth, we use stable contact areas and 2D projection masks to assess the HO-SGR task in the wild. We evaluate relevant methods and our approach preserves significantly higher stable contact area, on both EPIC-Grasps and stable grasp sub-sequences from the ARCTIC dataset.

Keywords: Hand-Object Reconstruction · 3D Reconstruction from Video · Egocentric Vision · Stable Grasp Dataset

1 Introduction

Accurately reconstructing three-dimensional hands along with a grasped or manipulated object is key to unlocking many perception problems, including fine-grained understanding of interactions, but also potential applications including augmented reality, robotic imitation learning and human-machine interactions.

Prior approaches have laid the foundation for the task, though focusing mostly on 3D input [2, 39, 49], which limits its application to the vast amount of video footage. Approaches with 2D input have relied on 3D ground truth for supervision [6, 18, 22, 46, 47], again restricting their scope to curated setups where multi-camera sensing and 3D ground truth can be obtained. Early insights [4, 18, 31] demonstrate that evaluation on in-the-wild egocentric footage remains significantly challenging.

In this work, we focus on the task of reconstruction in-the-wild on temporal periods of stable grasps. Our contribution is composed of three components.

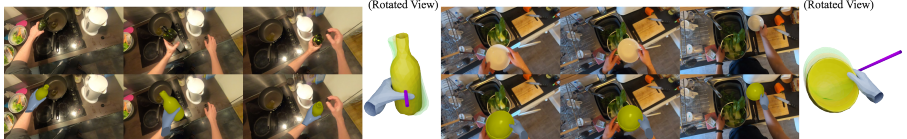


Fig. 1: Two stable grasp sequences from EPIC-Grasps for a bottle (left) and bowl (right). We show sample frames (top) and reconstructions (bottom). Right: for each reconstruction, we show the rotated view, along with the latent 1-DoF axis.

First, we propose the task of Hand-Object Stable Grasp Reconstruction (HO-SGR) which jointly optimises the reconstructions across all frames within one stable grasp. We showcase that objects move within one degree of freedom (1-DoF), relative to the hand pose, throughout the stable grasp. **Second**, we accordingly propose a method that jointly reconstructs the hands and objects by minimising the object’s motion, relative to the hand, to 1-DoF around a latent rotation axis, throughout the frames. We demonstrate our method outperforms baselines and alternative assumptions of object movement using 3D ground truth from the stable grasps within the egocentric views of the ARCTIC dataset [13]. **Third**, We label a sizeable dataset of 2.4K stable grasps clips from egocentric videos. Our EPIC-Grasps dataset is the first for hand-object reconstruction collected from unscripted activities, with individuals grasping 390 different objects by both hands. Similar to previous works [4, 5, 15, 17, 31], we restrict our evaluation to known category CAD models. Our dataset comes with pseudo-ground truth in the form of 2D segmentation masks available from [11], allowing to measure the 3D reconstruction’s projection relative to this 2D ground truth.

We evaluate our proposed method on EPIC-Grasps, outperforming other baselines using the proxy measure of stable grasps within 2D projections. We demonstrate that joint optimisation within the stable grasp is vital in the egocentric setup as finger joints are often concealed from the camera viewpoint introducing additional ambiguity when reconstructing from a single image.

We demonstrate a sample from our EPIC-Grasps dataset along with reconstructions from our method in Fig. 1.

2 Related Works

For comparison of hand object reconstruction datasets, see Sec. 4. We review related works in hand pose estimation and hand-object reconstruction.

3D Hand Pose Estimation. Estimating 3D hand pose from RGB images has been proposed for both free hands and hands in-interactions. FrankMocap [35] is commonly used CNN-based method and has been integrated into many hand-object reconstruction methods [4, 18, 31, 47, 48]. METRO [26] proposes to use a transformer on top of the CNN feature for regression. HaMeR [32] is a recent transformer-based method with improved training data scale and higher network capacity. A concurrent work, WildHands [33], addresses in-the-wild egocentric

hand pose estimation by considering perspective distortion and trains on relevant in-the-wild data. In this work, we use HaMeR [32] due to its superior performance. We also show HaMeR leads to better stable grasp reconstruction than FrankMocap in ablations.

3D Hand-Object-Reconstruction. Methods are grouped into two categories.

The first category, known-CAD methods, assumes that object CAD models are given and fits 3D shapes into 2D observations. These can further be classified into learning-based [1, 27, 40–42, 44, 46] or optimisation-based [4, 18, 31] methods. Learning-based methods learn to jointly reconstruct hands and objects from seen object examples, whereas optimisation-based methods address the reconstruction by directly fitting to 2D signals. RHO [4] is the first optimisation based single-frame method. The optimisation-based methods [4, 18, 31] share the same pipeline where hand/object is first independently optimised, followed by joint optimisation with physical terms. In particular, HOMan [18] is a generalisation of the single-frame method that incorporates temporal knowledge through the smoothness of mesh vertices over time and the temporal propagation of object pose initialisation.

The second category, CAD-agnostic methods, aims to estimate the hand and object poses without using explicit CAD models. Many CAD-agnostic methods [6, 19, 22, 47, 48] learn object shape priors from the data. The other line of methods [12, 16, 21] uses neural networks to fit the underlying object shape from multiple views. However, these methods typically require careful scanning of a held object, making them impractical for use in in-the-wild videos.

Our dataset and method belong to the first category, which is a simplified assumption needed for the challenges of in-the-wild reconstruction. Different from above optimisation-based methods, our approach examines the object’s relative motion and proposes to constrain the relative motion during stable grasp.

3 Stable Grasp Reconstruction: Problem and Method

We first define the standard task of hand-object reconstruction, then detail the adjustments we do to focus on stable grasps.

The general task of Hand-Object Reconstruction is defined as: given a sequence of N images of hand-object interactions, annotated with hand-side (left v.s. right) and a known object category, the task aims to produce, for every frame n , a pair of 3D meshes of the hand and the object w.r.t. the camera.

Different from the general task, we focus on a special temporal segment of object interactions – the **stable grasp** —which we will define in Sec 3.2. Given a start-end segment of a stable grasp, we aim to produce **consistent** hand object reconstructions across all frames within the stable grasp. We refer to this special-case task as Hand-Object Stable Grasp Reconstruction (HO-SGR).

3.1 Background and Notations

Following prior works [4, 18, 31], we use MANO [34] to represent the **hand mesh**, which takes as input a finger articulation vector $\theta \in \mathbb{R}^{45}$ and outputs the hand

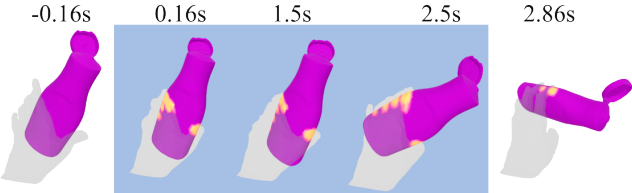


Fig. 2: Sample hand-object mesh sequence from ARCTIC. Contact areas (in shiny yellow) are similar within the stable grasp (blue background). In -0.16s the hand has no contact with the object.

mesh with vertices $V_h \in \mathbb{R}^{778 \times 3}$ in the *hand coordinate system*. We use the recent trained transformer model, HaMeR [32], to obtain the finger articulations θ^n from individual frames. We thus have per-frame hand vertices $V_h^n = \text{MANO}(\theta^n)$. Additionally, the hand-to-camera ($h2c$) pose $T_{h2c}^n \in SE(3)$ ¹, which is defined as the hand wrist orientation and position, is produced by HaMeR by default and are used to transform V_h^n to $V_{h:c}^n$ in the *camera coordinate system* for each frame.

For the **object mesh**, we use $V_o \in \mathbb{R}^{|V_o| \times 3}$ to denote the known object vertices in the *object coordinate system*. Different from [13, 18, 31], which estimates the object w.r.t. camera, we estimate the object-to-hand ($o2h$) poses $T_{o2h}^n \in SE(3)$ and the scalar scale $s \in \mathbb{R}$, which transforms object vertices to $V_{o:h}^n$ in the *hand coordinate system* for each frame. We then use the hand-to-camera ($h2c$) pose T_{h2c}^n to transform $V_{o:h}^n$ to $V_{o:c}^n$ in the *camera coordinate system* for each frame.

$$V_{o:c}^n = T_{h2c}^n(T_{o2h}^n(s * V_o)) \quad (1)$$

3.2 What is a *stable grasp (SG)*?

SG Definition. The term *stable grasp* has been previously used in human grasp analysis [3, 8, 14]. While definitions vary, they centre around the object being “held securely with one hand, irrespective of the hand orientation” [14]. Intuitively, this definition implies the hand maintains a stable contact (area) with the object – i.e. the same vertices of objects and hands are in contact for the duration of the grasp. For example, if a hand pours liquid out of a bottle, the hand indeed maintains contact with the same vertices in the bottle throughout manipulation, tilting to pour, then tilting back again upright before putting down. While the hand orientation and finger poses change during this interaction, the key here is the consistent stable contact area, which can be quantitatively computed from hand-object meshes. We visualise this example in Fig. 2.

Formally, for any pair of frames i and j within the stable grasp, we use S_i and S_j to denote the in-contact area on the object surface, and intersection-over-union IOU(S_i, S_j) between in-contact areas. Following above intuition, the

¹ $SE(3)$ denotes the space of all combinations of rotations and translations [30].

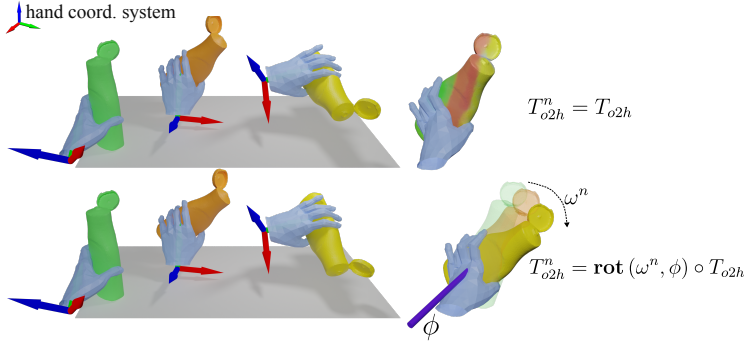


Fig. 3: To study the object’s relative pose, we align the hand coordinate systems (right). **Top:** Made-up sequence with static relative pose – object is perfectly aligned (mixture of 3 colours). **Bottom:** True sequence showcasing object’s motion relative to the hand can be approximated as 1-DoF rotation around axis ϕ , shown in purple.

duration of the stable grasp is defined as

$$[l^*, r^*] = \underset{l, r}{\operatorname{argmax}} (r - l) \quad \text{s.t. } \text{IOU}(S_i, S_j) > \tau \quad \forall l \leq i < j \leq r \quad (2)$$

where τ specifies the minimum IOU threshold. The $\operatorname{argmax}(r - l)$ implies the longest duration representing the stable grasp, from its initiation to conclusion.

SG Object Motion. It is critical to note that during the stable grasp, the hand still has dexterity to move or rotate an object relative to the hand pose; in other words, the object has non-static motions w.r.t. the hand. We visualise this distinction in Fig. 3 where we plot one manipulation sequence using two assumptions. The top assumes the object remains static relative to the hand pose – i.e. when the hand coordinate systems are aligned over the sequence, the object is perfectly aligned. This top example is actually a made-up one to explain the concept. The bottom example is a true sequence from the ARCTIC [13] dataset. We showcase that when the hand coordinate system is aligned over time, the object is visibly moving relative to the hand. The figure also shows that this motion is not completely free, but is restricted to rotation around a latent axis ϕ . This finding about the object’s motion during the stable grasp is one of our paper’s contributions. We detail next the study we carried out, which resulted in this finding.

SG Study. We perform a study on the 3D-ground-truth dataset ARCTIC [13] to analyse different quantitative measures within/outside the temporal extent of the stable grasp. We use the threshold $\tau = 0.5$ (Eq 2) and automatically extract 1303 stable grasp sequences from a variety of objects and subjects throughout dataset (see appendix for details).

We present the main finding in Fig 4. As anticipated, we show that the in-contact IOU, drops sharply outside the stable grasp – plotted in Fig 4 (left). That is the contact area remains stable only within the stable grasp’s temporal extent. We similarly compare other quantities (e.g. hand pose changes, fingertip pose variations and object rotation) within/outside stable grasps (details in

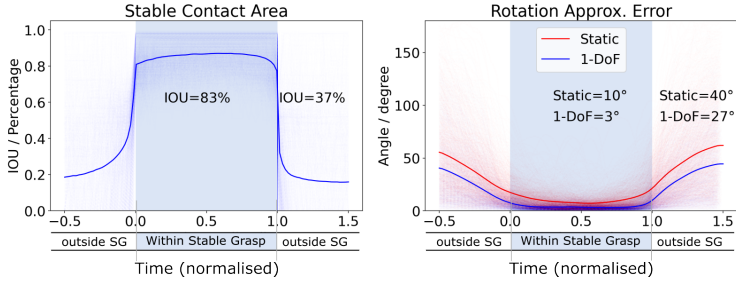


Fig. 4: We compare within/outside grasps, analysing object in-contact area (left) and corresponding rotation errors of the static and 1-DoF rotation approximations (right), normalising all stable grasp duration for direct comparison (0 to 1 marked with blue background). While both the Static and 1-DoF assumptions result in low approximation error within stable grasps, the error of 1-DoF assumption is marginal (right).

appendix). When we assess the **relative** object motion to the hand coordinate system within/outside the stable grasp, we note the findings first presented in Fig 3. Formally, we define a rotation axis ϕ around which the object can rotate – we detail how we find this axis later. If an object is only allowed to rotate around this axis, the motion is restricted from its free 6-DoF to a single rotation angle around this axis – we thus refer to this as a 1-DoF motion. The object pose w.r.t. the hand would then be described as

$$T_{o2h}^n = \text{rot}(\omega^n, \phi) \circ T_{o2h} \quad (3)$$

i.e., we first apply one global object-to-hand transform T_{o2h} for all frames, followed by applying the per-frame rotation $\text{rot}(\omega^n, \phi)$ – the rotation of angle ω^n around the given rotation axis ϕ . Here \circ denotes composition of transformations.

Given the ground truth hand and object poses across a sequence, we can find the optimal rotation axis ϕ by minimising the error between the predicted object-to-hand transformation and the ground truth ones, that is:

$$\underset{\phi, \{\omega^n\}, T_{o2h}}{\operatorname{argmin}} \frac{1}{N} \sum_{n=1}^N \|T_{o2h}^n - T_{gt}^n\|^2 \quad (4)$$

where T_{gt}^n is the ground truth object-to-hand transformation. In Fig. 4 (right) we plot this within/outside the temporal extent of stable grasp and compare that to the assumption that objects remain static (i.e. does not move relative to the hand). We calculate two rotation errors deviated from the ground truth – the first assumes the object remains static, and the second allows the object to move freely around ϕ and calculates the angle error off this axis. We show that the angle error when using the static assumption to be non-negligible (avg 10°). When we use the 1-DoF assumption, the error off the rotation axis ϕ is generally low (avg 3°).

In appendix, we further confirm these findings on the HOI4D [28] dataset. This finding on the object’s motion within the SG forms the base of our proposed optimisation for HO-SGR, which we present next.

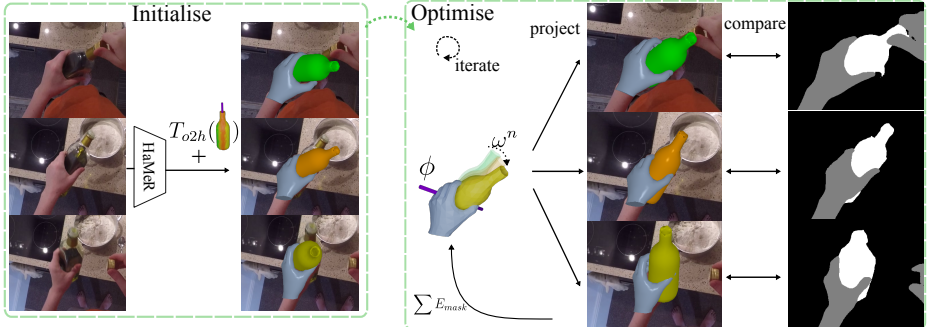


Fig. 5: Our proposed reconstruction method. We show 3 frames within a stable grasp. HaMeR [32] produces the hand meshes (rendered in blue) from RGB, and we set the object-to-hand pose T_{o2h} to the same T_{o2h} initially. Then, during each iteration of the optimisation, the object’s relative pose is optimised to 1-DoF and projected back to individual frames. These are compared with ground truth segmentation (right), jointly optimise for all frames. We ignore mask computation in hand occluded region (grey in the right figure). The physical terms are omitted in this figure.

3.3 Reconstructing Object Poses in a Stable Grasp

Recall that we aim to reconstruct the N pairs of 3D meshes of the hand and the object during the stable grasps. We use HaMeR [32] to reconstruct the hand pose individually in every frame. HaMeR is a fully transformer-based architecture of high accuracy and robustness, trained on very large scale hand data. Given an RGB image, HaMeR takes as input the hand detection bounding box with a known hand side, and outputs the MANO finger articulations θ^n and the hand-to-camera pose T_{h2c}^n .

We then reconstruct the object relative pose with the *render-and-compare* approach, overviewed in Fig. 5. We propose to leverage our finding on the stable grasp, to optimise the object pose relative to the hand. It is non-trivial to directly incorporate the stable contact area into the optimisation, as the contact area is not known in advance. Instead, we use our finding on the object relative motion, and minimise this to a single degree-of-freedom (1-DoF), i.e. the object rotates along a fixed latent axis to-be-optimised. As shown in Sec. 3.2, the 1-DoF object relative pose T_{o2h}^n at frame n is given by per-frame rotation ω^n , the rotation axis ϕ and the global base object-to-hand pose T_{o2h} that takes the object into the hand.

Our main objective function is given by:

$$E(\underbrace{\phi, \{\omega^n\}, T_{o2h}}_{\{T_{o2h}^n\}}, s; \{\theta^n\}, \{T_{h2c}^n\}) = \sum_{n=1}^N \lambda_1 E_{mask}^n + \lambda_2 E_{push}^n + \lambda_3 E_{pull}^n \quad (5)$$

where $\{\theta^n\}$ and $\{T_{h2c}^n\}$ are sets of outputs from HaMeR and are kept fixed, and s is the scalar object scale to be optimised.

We initialise the latent axis ϕ to the object’s z-axis from the CAD model; $\{\omega^n\}$ are initialised to zero. We note the initialisations for T_{o2h} in implementation details. We then jointly optimise all parameters across frames, in particular the rotation axis ϕ and the per-frame rotation angles $\{\omega^n\}$.

We use three terms in the optimisation: $E_{mask}^n, E_{push}^n, E_{pull}^n$. We describe these next. The main term E_{mask} focuses on estimating a reconstruction that best matches the 2D projections of the object masks throughout the sequence. We measure the error via sum of pixel differences:

$$E_{mask}^n = |\mathcal{C}_o^n \otimes (\mathcal{M}_o^n - \Pi(V_{o:c}^n))|_2^2 \quad (6)$$

where \mathcal{M}_o^n is the object mask which we use for supervision and $\Pi(\cdot)$ is the differentiable projection function [23]. \mathcal{C}_o^n is the occlusion-aware mask as in [18, 50] which only computes the error within regions of the object that are not occluded by the hand, set to 1 for the object and the background, and 0 for the hand. This masking is critical to avoid penalising the missing parts of the object mask due to in-hand occlusion.

We also employ two additional terms, used in previous works [4, 18, 31, 46]. We use the physical heuristics E_{push} , which pushes the object out of the penetrating region against the hand and a balancing loss E_{pull} which pulls the object to touch these contact regions. For exact calculations of these previously used physical heuristics terms, refer to the appendix.

4 EPIC-Grasps Annotations

With the definition of stable grasp in Sec 3.2, we now use this to annotate the temporal extents of stable grasps in unscripted egocentric recordings capturing in-the-wild hand-object stable grasps. This offers a dataset distinct from prior works, where frame-level labels [4, 19, 45], 3D supervision [2, 39, 49] or recordings specifically collected to evaluate grasps with no underlying action [5, 17, 25] are typically used. Instead, we aim to find stable grasps from within egocentric videos recorded of daily actions in an unscripted manner.

We next detail our pipeline to annotate EPIC-Grasps:

1. Identifying candidate clips to annotate. The ultimate goal of hand-object reconstruction is to operate for any rigid or dynamic objects, including novel classes. However, current approaches for reconstruction of unknown objects are still in their infancy [21, 37, 38, 47, 48] (we show failure cases in appendix). We thus restrict our first-attempt at reconstructing stable grasps in-the-wild to objects of a known category. Note that this is distinct from instance CAD models – the general CAD model of a bottle might not exactly match all bottles in daily life. We exclude very small objects and shortlist 9 object categories frequently used in kitchens: plate, bowl, bottle, cup, mug, can, pan, saucepan, glass².

We begin with the frame-level hand-object interaction annotations from VISOR [11], in which we identified clips where the a hand is in contact with one of

² For the **object mesh**, we made one category CAD model in Blender [7].

Dataset	Year	Characteristics			Stats					Labels	
		In-the-wild	Funct. Intent	Ego	#Env	#Sub	#Cat	#Inst	#Seq	Pose GT	Stable Grasp
FPHA [15]	2018	✗	✓	✓	3	6	4	4	1,175	3D	✗
HO3D [17]	2020	✗	✗	✗	1	10	10	10	65	3D	✓(part)
ContactPose [2]	2020	✗	✓	✗	1	50	25	25	2,306	3D	✓
GRAB [39]	2020	✗	✓	✗	1	10	51	51	1,334	3D	✗
H2O [25]	2021	✗	✓	✓	3	4	8	8	24	3D	✗
DexYCB [5]	2021	✗	✗	✗	1	10	20	20	1,000	3D	✗
HOI4D [28]	2022	✗	✓	✓	610	9	20	800	5,000	3D	✗
Assembly101 [36]	2022	✗	✓	✗	1	53	15	15	4,321	3D Hand*	✗
OakInk [45]	2022	✗	✓	✗	1	12	32	100	1,356	3D	✗
ARCTIC [13]	2023	✗	✓	✓	1	9 [†]	11	11	339	3D	✗
ARCTIC-Grasps (ours)	2024	✗	✓	✓	1	9	11	11	1,303	3D	✓
Core50 [29]	2017	✓	✗	✗	11	-	10	50	550	2D Mask	✗
MOW [4, 31]	2021	✓	✓	✗	500	500	121	500	500	✗	✗
EPIC-Grasps (ours)	2024	✓	✓	✓	141	31	9	~390	2,431	2D Mask	✓

Table 1: Dataset Comparison: *: cannot be used for hand-object reconstruction as object poses or segments are not provided. [†]: subjects in the released train/val set.

the categories above. The annotations also inform us which hand is in contact with the object (i.e. left or right). We then use the fine-grained action labels available from EPIC-KITCHENS [9, 10] to locate the initial temporal extent for actions involving any of these categories.

2. Annotating Stable Grasps. Two annotators were asked to label the start-and-end frames following the stable grasp definition. We discard segments when (i) a segment does not contain any stable grasp (ii) both the hand and object are out-of-view during the sequence or (iii) the object does not match the category CAD model specified.

3. 2D Hand and Object Segmentation Annotations. In total, we label 2431 video clips of stable grasps from 141 distinct videos in 31 kitchens [10]. For each clip, we provide a start and end time of the stable grasp, as well as 319,661 segmentation masks for the hand and the object during the stable grasp from the dense VISOR annotations [11]. Of these, 1446 contain left hand stable grasps and 985 contain right hand stable grasps. Note that the majority of subjects recording the EPIC-KITCHENS dataset are right-handed—which implies the left hand is more frequently used to steady the object during manipulation. Compared to previous efforts [5, 17, 25, 28, 38], most clips in EPIC-Grasps contains *both hands in view* manipulating the same or different objects. We provide the breakdown per category and grasp duration in appendix.

Tab. 1 compares our dataset with currently available and regularly used datasets for hand-object reconstruction. In the first section, we show datasets collected with 3D ground truth and add the 1303 stable grasp sequences previously noted in Sec. 3.2. We refer to these as ARCTIC-Grasps. We note that previous datasets, including those that requiring 3D ground truth, are limited in the environmental setup to allow for multi-camera views or motion capture tracking. This limits the appearance diversity and interactions are not functional. In Tab. 1 we also report the functional intent of various dataset (i.e. object is used with intent). EPIC-Grasps is the first to capture in-the-wild egocentric videos with functional intent. Of particular note is the HOI4D [28] where diversity is

targeted with a large number of indoor rooms. However, this is a constructed setup, where objects are selected from a given pool. In EPIC-Grasps, subjects are recording in their personal kitchens and using their chosen objects as part of longer activities.

5 Experiments

The experiment section is structured as follows: in Sec. 5.1 and Sec. 5.2 we describe the implementation details of our method and the quantitative metrics respectively. Sec. 5.3 and Sec. 5.4 report results of our method and baselines on ARCTIC-Grasps and EPIC-Grasps, respectively. Finally Sec. 5.5 conducts ablation studies on our method.

5.1 Implementation Details

We follow the convention in HOMan [18] which sparsely and linearly samples 30 frames from the sequence for optimisation and evaluation. We use 50 initialisations of object rotation and 1 global translation for each object, from ground truth of ARCTIC to find these initialisations, following [18]. The optimisation process takes 1.5 minutes on a 2080Ti for one 30-frame sequence on average.

The error E_{mask} is defined in pixels whilst E_{push} and E_{pull} are defined in 3D space (mm), and are related by the camera’s focal length f . We introduce a focal scaling factor: $\lambda_f = f * \text{render_size}$. We use `render_size` = 256 and set $\lambda_1 = 1$, $\lambda_2 = 0.1 * \lambda_f$ and $\lambda_3 = 0.1 * \lambda_f$; here the focal length f is estimated by HaMeR [32]. Please refer to appendix for further implementation details.

5.2 Baselines and Quantitative Metrics

We focus on baselines that do not require training on the dataset in advance. We thus use 4 baselines to compare to:

- **HOMan** [18]—a common CAD-based baseline that progressively optimises the object pose relative to the hand. We use the ground truth masks as in our method for fair comparison.
- **Single Frame**—We predict the hand and object meshes independently for each frame, without utilising any temporal optimisation or the knowledge of stable grasps.
- **Static**—A version of our method where objects are not allowed any motion when within the stable grasp, minimising the overall rotation and translation of the object.
- **Dynamic**—A variation of our method where objects are allowed to move freely within 6-Dof.

We note that RHOV [31] does not have released code to be used as a baseline.

We propose quantitative metrics to measure the correctness of the predicted object poses within the stable grasp. Given the knowledge that stable grasps

Category	Single Frame			HOMAN [18]			Static			Dynamic			1-DoF							
	IOU	SCA	IOU ADD SCA-ADD	IOU	SCA	IOU ADD SCA-ADD	IOU	SCA	IOU ADD SCA-ADD	IOU	SCA	IOU ADD SCA-ADD	IOU	SCA	IOU ADD SCA-ADD					
box	93.2	17.5	9.4	3.1	83.5	30.9	33.3	16.9	90.9	67.3	37.7	28.7	95.2	41.7	57.2	25.4	94.2	56.7	39.1	23.6
capsulemachine	79.3	17.8	8.4	3.3	84.0	34.4	42.1	24.5	79.8	34.9	48.4	34.1	88.8	41.6	53.7	29.2	86.1	51.4	62.1	41.2
espressomachine	82.8	19.1	22.8	8.3	84.2	36.9	44.6	28.8	82.6	49.2	48.5	36.2	89.6	43.1	66.3	34.5	87.4	54.9	54.5	35.6
ketchup	81.3	29.3	30.2	16.4	72.0	18.0	15.1	9.3	75.3	32.7	51.9	37.8	89.4	56.0	62.3	40.2	84.0	55.4	64.2	45.0
laptop	87.8	24.9	16.7	7.0	82.1	35.3	43.8	28.0	86.0	62.0	45.1	37.1	93.3	50.2	63.2	34.6	91.4	68.0	54.9	40.8
microwave	85.7	17.1	29.5	8.0	87.0	36.1	56.2	27.3	85.4	51.5	50.9	35.3	90.3	35.2	53.6	23.0	89.0	52.5	55.4	34.8
mixer	79.4	12.1	14.8	4.9	85.3	34.3	45.1	26.7	79.3	37.9	48.4	32.2	89.1	38.4	59.0	29.0	87.0	52.0	62.3	39.6
notebook	87.2	25.6	6.6	2.8	85.7	38.7	33.8	20.8	84.5	57.8	43.0	33.2	93.5	52.8	63.6	35.0	90.9	65.5	55.6	38.7
phone	82.9	25.7	15.1	6.8	80.9	39.5	28.1	19.9	77.8	36.7	39.7	29.2	91.1	58.8	37.7	23.5	88.1	61.9	54.1	37.6
scissors	48.5	0.0	14.0	9.3	40.9	5.2	7.0	5.2	48.2	0.0	47.4	36.3	73.9	18.2	56.1	38.9	62.4	2.7	68.4	51.8
waffleiron	85.7	13.1	3.1	0.9	86.5	36.3	45.0	26.2	84.7	48.3	59.5	39.2	92.7	44.3	81.7	38.1	91.2	55.9	69.5	43.7
All	83.3	19.5	15.0	6.0	81.4	33.1	37.1	22.0	81.4	46.6	46.9	34.2	90.8	45.5	59.6	31.5	88.1	55.7	57.3	38.5

Table 2: Results on ARCTIC-Grasps. Green shows the best performing method per metric and yellow shows the second best.

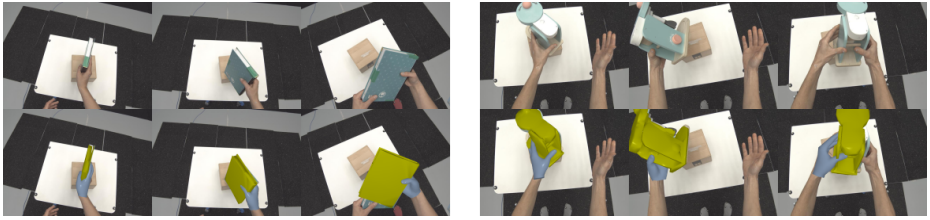


Fig. 6: Two stable grasp reconstructions by 1-DoF method on ARCTIC-Grasps.

maintain a consistent contact area between the hand and the object throughout the sequence, we measure this contact area over time. However, a reconstruction can maintain a stable contact area but be completely erroneous. We thus propose to combine a measure of correctness of reconstruction with the stability of the contact area to produce a robust metric. We explain this next.

Average Distance (ADD %). Following [20, 24, 43], we measure the distance of corresponding vertices between GT and predicted object vertices in the hand coordinate system, and average this distance over vertices and frames. ADD is 1 for a sequence if the average distance is less than 10% of the object’s diameter, and 0 otherwise.

Average Stable Contact Area at ADD Success (SCA-ADD %). When a pose is considered correct for a sequence, i.e. ADD is 1, we measure the stable contact area across the sequence, defined as the average IOU of in contact area between each pair of frames (Sec. 3.2). SCA-ADD is set to 0 when ADD is set to 0 (average distance below threshold). We average SCA-ADD over all examples.

Intersection-over-Union (IOU %). We use IOU as a proxy of pose accuracy when 3D GT is not available. We measure the Intersection-over-Union between the ground truth mask and the rendered mask for the object in camera view. We report average IOU across all frames. Due to occlusion with other components in the scene, only the non-occluded area of the rendered projection is used.

Average Stable Contact Area at high IOU (SCA-IOU %). Using IOU as proxy for correct reconstructions, we analogously report SCA when IOU is more than certain thresholds. We use 80% as threshold on ARCTIC-Grasps and report both 80% and 60% on EPIC-Grasps. SCA-IOU is set to 0 when IOU is below the threshold. We report average SCA-IOU.

Category	HOMan [18]			Dynamic			1-DoF		
	IOU	SCA@0.8	SCA@0.6	IOU	SCA@0.8	SCA@0.6	IOU	SCA@0.8	SCA@0.6
bottle	56.7	3.4	5.8	75.5	21.8	36.6	72.1	26.1	51.3
bowl	54.4	1.1	1.6	58.0	9.3	19.8	56.2	11.1	25.7
can	48.3	3.4	5.1	56.0	13.7	20.1	54.1	16.5	26.6
cup	56.9	5.5	7.8	67.5	16.5	38.9	65.9	18.4	46.1
glass	55.4	3.0	4.2	65.2	14.8	30.1	62.5	15.7	37.8
mug	59.4	3.9	6.6	63.8	6.3	29.6	62.6	10.8	38.6
pan	48.3	0.5	1.9	48.9	4.3	12.8	49.1	7.0	20.4
plate	61.1	1.0	1.6	68.1	17.6	30.1	65.2	16.3	34.6
saucepans	51.1	0.4	2.4	57.5	5.4	25.7	56.8	8.5	34.6
All	54.9	1.9	3.3	61.7	12.2	25.3	59.9	14.1	32.9

Table 3: Results on EPIC-Grasps. Green for best and yellow shows the second best.

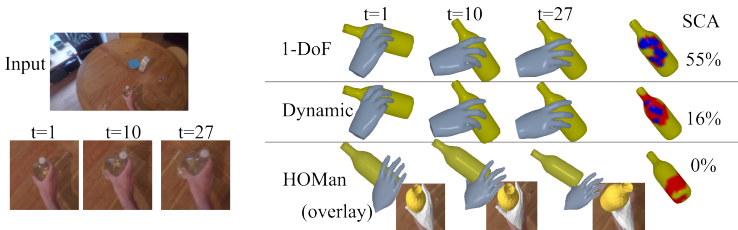


Fig. 7: Qualitative comparison between 1-DoF, Dynamic and HOMan [18] on EPIC-Grasps. We show input frames, reconstruction results and the corresponding SCA.

The first two metrics, ADD and SCA-ADD, are evaluated when 3D ground truths are available—e.g. ARCTIC-Grasps dataset; and the other two are the corresponding 2D proxy, which we use for EPIC-Grasps.

5.3 Results on ARCTIC-Grasps

Tab. 2 compares results on ARCTIC-Grasps, using all the metrics. We here focus on the object metrics, using ground truth hand mesh and a known object scale. Whilst Dynamic and 1-DoF both have significantly higher ADD results, 1-DoF maintains the best SCA when grasps are successfully reconstructed (high SCA-ADD). Static has considerably high SCA, but IOU and ADD are significantly lower than 1-DoF in every category. HOMan only performs best on the “microwave” object sequences. Single Frame performs worst in every case. We show qualitative examples in Fig. 6.

5.4 Results on EPIC-Grasps

Tab. 3 compares results on EPIC-Grasps dataset using proxy metrics IOU and SCA-IOU at two thresholds (0.8 and 0.6). We compare 1-DoF to the best variation from ARCTIC-Grasps: Dynamic. 1-DoF achieves the best SCA-IOU metric for both thresholds for every object category and overall.

Fig. 7 shows comparative results. Despite acceptable overlay, HOMan does not maintain the stable grasp and the object is in fact sliding in the hand over



Fig. 8: Qualitative Results on EPIC-Grasps (3 examples/ category); projected reconstruction results and reconstruction in rotated views. Bottom: failure cases due to wrong hand pose (left), extreme occlusion (mid) and limited views (right).

time. The Dynamic baseline has significantly lower SCA with the contact area drifting over time. Our proposed 1-DoF method is able to reconstruct the stable grasp as it benefits from the constrained relative pose assumption.

Fig. 8 shows reconstruction results of our 1-DoF approach on the EPIC-Grasps dataset. We showcase three examples per category. From the images, the challenge in EPIC-Grasps is evident with the hand and object occupying a small proportion of the image. In most examples, the palm and fingers are concealed. Importantly, all grasps are functional – e.g. picking a cup from the drainer.

5.5 Ablation Studies

In this section, we ablate the hand pose estimator and loss functions under the in-the-wild setting, on full EPIC-Grasps dataset. The 1-DoF assumption of the method has been ablated against other variants in Tab. 2.

Ablation on the hand pose estimation method. In Tab. 4, we compare HaMeR against FrankMocap [35], a commonly used hand predictor in other works [4, 18, 31]. HaMeR consistently outperforms the results with FrankMocap on all metrics, which is in line with the higher capacity of HaMeR over FrankMocap. We include a detailed table in appendix.

Ablation on physical terms E_{push} and E_{pull} . In Tab. 5, we ablate the physical terms E_{push} and E_{pull} introduced in the loss function Eq. (5). Note that while removing physical terms ($\lambda_2 = \lambda_3 = 0$) slightly improves IOU and SCA@0.8, it significantly decreases SCA@0.6 by 5.4%.

Method	IOU	SCA@0.8	SCA@0.6
1-DoF + FrankMocap [35]	55.1	7.2	20.3
1-DoF + HaMeR [32]	59.9	14.1	32.9

Table 4: Ablation on the hand pose estimator.

λ_2	λ_3	IOU	SCA@0.8	SCA@0.6
0.0	0.0	62.5	15.1	27.5
0.1	0.1	59.9	14.1	32.9
1.0	1.0	53.4	12.2	25.3

Table 5: Ablation on the physical terms. We highlight our choice of λ_2 and λ_3 (blue).

\mathcal{C}_o^n	IOU	SCA@0.8	SCA@0.6
✗	51.0	3.5	20.4
✓	59.9	14.1	32.9

Table 6: Ablation on occlusion-aware mask \mathcal{C}_o^n .

Ablation on Occlusion Mask. In Tab. 6, we show that using \mathcal{C}_o^n is critical in the optimisation, whereas removing \mathcal{C}_o^n drastically reduces the results.

5.6 Limitations

Whilst results in-the-wild are very promising, our pipeline relies on HaMeR as a first stage. Despite the robustness incorporated by the multiple-view joint optimisation, our method fails when the predicted hand poses are wrong (see Fig. 8). Our method also struggle with extreme occlusions and ambiguity from limited views. The 1-DoF assumption also relies on the knowledge of stable grasp duration, which is liable to fail outside grasps.

Another limitation of our approach is its reliance on the knowledge of the category’s CAD model. Current CAD-agnostic methods [47] struggle in-the-wild – we showcase failures in appendix. However, removing the limitation of CAD model knowledge is a clear future direction.

6 Conclusion

In this paper we propose the task of hand-object stable grasp reconstruction. By focusing on stable grasps, we can jointly optimise multiple frames given the knowledge of how objects move relative to the hand within grasp. We further build a challenging in-the-wild egocentric videos dataset for the task. The dataset contains 2D masks as pseudo ground truths and manual temporal labels of stable grasps. We evaluate the method’s ability without 3D ground truth by measuring the 2D IOU of object masks along with measuring the stable contact area over time. We show that the constrained object motion achieves better hand-object reconstructions within the stable grasp.

By investigation stable grasps, we hope to encourage more works to quantitatively evaluate methods in-the-wild.

Acknowledgements. Research is supported by EPSRC UMPIRE (EP/T004991/1). Z. Zhu is supported by UoB-CSC Scholarship.

References

1. Aboukhadra, A.T., Malik, J., Elhayek, A., Robertini, N., Stricker, D.: Thor-net: End-to-end graformer-based realistic two hands and object reconstruction with self-supervision. In: Proceedings of the IEEE/CVF Winter Conference on Applications of Computer Vision. pp. 1001–1010 (2023) [3](#)
2. Brahmbhatt, S., Tang, C., Twigg, C.D., Kemp, C.C., Hays, J.: Contactpose: A dataset of grasps with object contact and hand pose. In: Proceedings of the European Conference on Computer Vision (ECCV). pp. 361–378 (2020) [1](#), [8](#), [9](#)
3. Bullock, I.M., Ma, R.R., Dollar, A.M.: A hand-centric classification of human and robot dexterous manipulation. *IEEE Transactions on Haptics* **6**(2), 129–144 (2013) [4](#)
4. Cao, Z., Radosavovic, I., Kanazawa, A., Malik, J.: Reconstructing hand-object interactions in the wild. In: Proceedings of the IEEE/CVF International Conference on Computer Vision. pp. 12417–12426 (2021) [1](#), [2](#), [3](#), [8](#), [9](#), [13](#)
5. Chao, Y.W., Yang, W., Xiang, Y., Molchanov, P., Handa, A., Tremblay, J., Narang, Y.S., Van Wyk, K., Iqbal, U., Birchfield, S., et al.: Dexycb: A benchmark for capturing hand grasping of objects. In: Proceedings of the IEEE/CVF Conference on Computer Vision and Pattern Recognition. pp. 9044–9053 (2021) [2](#), [8](#), [9](#)
6. Chen, Z., Hasson, Y., Schmid, C., Laptev, I.: Alignsdf: Pose-aligned signed distance fields for hand-object reconstruction. In: Proceedings of the European Conference on Computer Vision (ECCV). pp. 231–248 (2022) [1](#), [3](#)
7. Community, B.O.: Blender - a 3D modelling and rendering package. Blender Foundation, Stichting Blender Foundation, Amsterdam (2018), <http://www.blender.org> [8](#)
8. Cutkosky, M.: On grasp choice, grasp models, and the design of hands for manufacturing tasks. *IEEE Transactions on Robotics and Automation* **5**(3), 269–279 (1989) [4](#)
9. Damen, D., Doughty, H., Farinella, G.M., Fidler, S., Furnari, A., Kazakos, E., Moltisanti, D., Munro, J., Perrett, T., Price, W., et al.: Scaling egocentric vision: The epic-kitchens dataset. In: Proceedings of the European Conference on Computer Vision (ECCV). pp. 720–736 (2018) [9](#)
10. Damen, D., Doughty, H., Maria Farinella, G., , Furnari, A., Ma, J., Kazakos, E., Moltisanti, D., Munro, J., Perrett, T., Price, W., Wray, M.: Rescaling egocentric vision: Collection, pipeline and challenges for epic-kitchens-100. *International Journal of Computer Vision (IJCV)* **130**, 33–55 (2022) [9](#)
11. Darkhalil, A., Shan, D., Zhu, B., Ma, J., Kar, A., Higgins, R., Fidler, S., Fouhey, D., Damen, D.: Epic-kitchens visor benchmark: Video segmentations and object relations. In: Proceedings of the Neural Information Processing Systems (NeurIPS) Track on Datasets and Benchmarks (2022) [2](#), [8](#), [9](#)
12. Fan, Z., Parelli, M., Kadoglou, M.E., Kocabas, M., Chen, X., Black, M.J., Hilliges, O.: HOLD: Category-agnostic 3d reconstruction of interacting hands and objects from video. In: Proceedings IEEE Conference on Computer Vision and Pattern Recognition (2024) [3](#), [22](#)
13. Fan, Z., Taheri, O., Tzionas, D., Kocabas, M., Kaufmann, M., Black, M.J., Hilliges, O.: ARCTIC: A dataset for dexterous bimanual hand-object manipulation. In: Proceedings IEEE Conference on Computer Vision and Pattern Recognition (2023) [2](#), [4](#), [5](#), [9](#), [19](#)
14. Feix, T., Romero, J., Schmiedmayer, H.B., Dollar, A.M., Kräig, D.: The GRASP Taxonomy of Human Grasp Types. *IEEE Transactions on Human-Machine Systems* **46**(1), 66–77 (2016) [4](#)

15. Garcia-Hernando, G., Yuan, S., Baek, S., Kim, T.: First-person hand action benchmark with RGB-D videos and 3d hand pose annotations. In: Proceedings of the IEEE Conference on Computer Vision and Pattern Recognition. pp. 409–419 (2018) 2, 9
16. Hampali, S., Hodan, T., Tran, L., Ma, L., Keskin, C., Lepetit, V.: In-hand 3d object scanning from an rgb sequence. In: Proceedings IEEE Conference on Computer Vision and Pattern Recognition (2023) 3
17. Hampali, S., Rad, M., Oberweger, M., Lepetit, V.: Honnoteate: A method for 3d annotation of hand and object poses. In: Proceedings of the IEEE/CVF Conference on Computer Vision and Pattern Recognition. pp. 3193–3203 (2020) 2, 8, 9, 22
18. Hasson, Y., Varol, G., Schmid, C., Laptev, I.: Towards unconstrained joint hand-object reconstruction from rgb videos. In: 2021 International Conference on 3D Vision (3DV). pp. 659–668 (2021) 1, 2, 3, 4, 8, 10, 11, 12, 13, 23, 24
19. Hasson, Y., Varol, G., Tzionas, D., Kalevatykh, I., Black, M.J., Laptev, I., Schmid, C.: Learning joint reconstruction of hands and manipulated objects. In: Proceedings of the IEEE Conference on Computer Vision and Pattern Recognition. pp. 11807–11816 (2019) 3, 8
20. Hodan, T., Barath, D., Matas, J.: EPOS: Estimating 6d pose of objects with symmetries. In: Proceedings of the IEEE/CVF Conference on Computer Vision and Pattern Recognition. pp. 11703–11712 (2020) 11
21. Huang, D., Ji, X., He, X., Sun, J., He, T., Shuai, Q., Ouyang, W., Zhou, X.: Reconstructing Hand-Held Objects from Monocular Video. In: Proceedings of SIGGRAPH Asia 2022 Conference Papers (2022) 3, 8, 22
22. Karunratanakul, K., Yang, J., Zhang, Y., Black, M.J., Muandet, K., Tang, S.: Grasping field: Learning implicit representations for human grasps. In: 2020 International Conference on 3D Vision (3DV). pp. 333–344 (2020) 1, 3
23. Kato, H., Ushiku, Y., Harada, T.: Neural 3d mesh renderer. In: Proceedings of the IEEE Conference on Computer Vision and Pattern Recognition. pp. 3907–3916 (2018) 8
24. Krull, A., Brachmann, E., Michel, F., Yang, M.Y., Gumhold, S., Rother, C.: Learning analysis-by-synthesis for 6d pose estimation in rgb-d images. In: Proceedings of the IEEE International Conference on Computer Vision. pp. 954–962 (2015) 11
25. Kwon, T., Tekin, B., Stühmer, J., Bogo, F., Pollefeys, M.: H2o: Two hands manipulating objects for first person interaction recognition. In: Proceedings of the IEEE/CVF International Conference on Computer Vision. pp. 10138–10148 (2021) 8, 9
26. Lin, K., Wang, L., Liu, Z.: End-to-end human pose and mesh reconstruction with transformers. In: Proceedings of the IEEE/CVF Conference on Computer Vision and Pattern Recognition (2021) 2
27. Liu, S., Jiang, H., Xu, J., Liu, S., Wang, X.: Semi-supervised 3d hand-object poses estimation with interactions in time. In: Proceedings of the IEEE/CVF Conference on Computer Vision and Pattern Recognition. pp. 14687–14697 (2021) 3
28. Liu, Y., Liu, Y., Jiang, C., Lyu, K., Wan, W., Shen, H., Liang, B., Fu, Z., Wang, H., Yi, L.: Hoi4d: A 4d egocentric dataset for category-level human-object interaction. In: Proceedings of the IEEE/CVF Conference on Computer Vision and Pattern Recognition. pp. 21013–21022 (2022) 6, 9, 20
29. Lomonaco, V., Maltoni, D.: Core50: a new dataset and benchmark for continuous object recognition. In: Conference on Robot Learning. pp. 17–26 (2017) 9
30. Ma, Y., Soatto, S., Kosecka, J., Sastry, S.S.: An Invitation to 3-D Vision: From Images to Geometric Models. SpringerVerlag (2003) 4

31. Patel, A., Wang, A., Radosavovic, I., Malik, J.: Learning to imitate object interactions from internet videos. arXiv preprint arXiv:2211.13225 (2022) [1](#), [2](#), [3](#), [4](#), [8](#), [9](#), [10](#), [13](#)
32. Pavlakos, G., Shan, D., Radosavovic, I., Kanazawa, A., Fouhey, D., Malik, J.: Reconstructing hands in 3d with transformers. In: Proceedings of the IEEE/CVF Conference on Computer Vision and Pattern Recognition (2024) [2](#), [3](#), [4](#), [7](#), [10](#), [14](#), [22](#)
33. Prakash, A., Tu, R., Chang, M., Gupta, S.: 3d hand pose estimation in egocentric images in the wild. arXiv **2312.06583** (2023) [2](#)
34. Romero, J., Tzionas, D., Black, M.J.: Embodied Hands: Modeling and Capturing Hands and Bodies Together. ACM Trans. Graph **36**, 17 (2017) [3](#)
35. Rong, Y., Shiratori, T., Joo, H.: Frankmocap: A monocular 3d whole-body pose estimation system via regression and integration. In: Proceedings of the IEEE/CVF International Conference on Computer Vision Workshop. pp. 1749–1759 (2021) [2](#), [13](#), [14](#), [22](#), [23](#)
36. Sener, F., Chatterjee, D., Shelepov, D., He, K., Singhania, D., Wang, R., Yao, A.: Assembly101: A large-scale multi-view video dataset for understanding procedural activities. In: Proceedings of the IEEE/CVF Conference on Computer Vision and Pattern Recognition. pp. 21096–21106 (2022) [9](#)
37. Sucar, E., Wada, K., Davison, A.: NodeSLAM: Neural Object Descriptors for Multi-View Shape Reconstruction. In: Proceedings of the International Conference on 3D Vision (3DV) (2020) [8](#)
38. Swamy, A., Leroy, V., Weinzaepfel, P., Baradel, F., Galaoui, S., Brégier, R., Armando, M., Franco, J.S., Rogez, G.: Showme: Benchmarking object-agnostic hand-object 3d reconstruction. In: Proceedings of the IEEE/CVF International Conference on Computer Vision Workshop. pp. 1935–1944 (2023) [8](#), [9](#)
39. Taheri, O., Ghorbani, N., Black, M.J., Tzionas, D.: Grab: A dataset of whole-body human grasping of objects. In: Proceedings of the European Conference on Computer Vision (ECCV). pp. 581–600 (2020) [1](#), [8](#), [9](#)
40. Tekin, B., Bogo, F., Pollefeys, M.: H+O: unified egocentric recognition of 3d hand-object poses and interactions. In: Proceedings of the IEEE Conference on Computer Vision and Pattern Recognition. pp. 4511–4520 (2019) [3](#)
41. Tse, T.H.E., Kim, K.I., Leonardis, A., Chang, H.J.: Collaborative learning for hand and object reconstruction with attention-guided graph convolution. In: Proceedings of the IEEE/CVF Conference on Computer Vision and Pattern Recognition. pp. 1664–1674 (2022) [3](#)
42. Wang, R., Mao, W., Li, H.: Interacting hand-object pose estimation via dense mutual attention. In: Proceedings of the IEEE/CVF Winter Conference on Applications of Computer Vision. pp. 5735–5745 (2023) [3](#)
43. Xiang, Y., Schmidt, T., Narayanan, V., Fox, D.: Posecnn: A convolutional neural network for 6d object pose estimation in cluttered scenes. arXiv preprint arXiv:1711.00199 (2017) [11](#)
44. Yang, L., Li, K., Zhan, X., Lv, J., Xu, W., Li, J., Lu, C.: Artiboost: Boosting articulated 3d hand-object pose estimation via online exploration and synthesis. In: Proceedings of the IEEE/CVF Conference on Computer Vision and Pattern Recognition. pp. 2750–2760 (2022) [3](#)
45. Yang, L., Li, K., Zhan, X., Wu, F., Xu, A., Liu, L., Lu, C.: Oakink: A large-scale knowledge repository for understanding hand-object interaction. In: Proceedings of the IEEE/CVF Conference on Computer Vision and Pattern Recognition. pp. 20953–20962 (2022) [8](#), [9](#)

46. Yang, L., Zhan, X., Li, K., Xu, W., Li, J., Lu, C.: Cpf: Learning a contact potential field to model the hand-object interaction. In: Proceedings of the IEEE/CVF International Conference on Computer Vision. pp. 11097–11106 (2021) [1](#), [3](#), [8](#)
47. Ye, Y., Gupta, A., Tulsiani, S.: What’s in your hands? 3d reconstruction of generic objects in hands. In: Proceedings of the IEEE/CVF Conference on Computer Vision and Pattern Recognition. pp. 3895–3905 (2022) [1](#), [2](#), [3](#), [8](#), [14](#), [22](#), [23](#)
48. Ye, Y., Hebbar, P., Gupta, A., Tulsiani, S.: Diffusion-guided reconstruction of everyday hand-object interaction clips. In: Proceedings of the IEEE/CVF International Conference on Computer Vision. pp. 19717–19728 (2023) [2](#), [3](#), [8](#), [22](#)
49. Zhang, H., Ye, Y., Shiratori, T., Komura, T.: ManipNet: Neural Manipulation Synthesis with a Hand-Object Spatial Representation. ACM Transactions on Graphics **40**(4) (2021) [1](#), [8](#)
50. Zhang, J.Y., Pepose, S., Joo, H., Ramanan, D., Malik, J., Kanazawa, A.: Perceiving 3d human-object spatial arrangements from a single image in the wild. In: Proceedings of the European Conference on Computer Vision (ECCV). pp. 34–51 (2020) [8](#)

Appendix

This appendix is structured as follows: Appendix **A** presents statistics of EPIC-Grasps annotation. Appendix **B** presents statistics of ARCTIC-Grasps annotation. Appendix **C** provides the stable grasp study on ARCTIC and HOI4D dataset. Appendix **D** showcases failure of current CAD-agnostic approach on EPIC-Grasps dataset. Appendix **E** provides ablation of the hand pose estimation method. Appendix **F** provides further implementation details.

A Statistics of EPIC-Grasps annotation

In Table 7, we present average, standard deviation and maximum clip duration for each of our categories as well as the total number of video clips per category in EPIC-Grasps. Note that grasping some categories (e.g. pan) can be significantly longer in duration than others (e.g. mug).

B Statistics of ARCTIC-Grasps automatic annotation

We use Eq (2) in the main paper to automatically extract stable grasp duration from the 3D ARCTIC [13] dataset, where in-contact area can be computed from ground truth meshes. We set τ to 0.5 empirically: we inspect the resulting grasps to ensure the start-end time match visual expectation. As our pipeline assumes rigid object, we exclude segments where the hand is changing the object’s articulation.

In Table 8, we present average, standard deviation and maximum clip duration for each category as well as total number of video clips per category in ARCTIC-Grasps. As ARCTIC sequences do not include actual activities (e.g. a box is opened only to be closed again rather than to retrieve something from inside), the stable grasps are shorter than those in the unscripted functional recordings of EPIC-Grasps.

C Stable Grasp Study on ARCTIC and HOI4D datasets.

In this section, we analyse metrics related to stable grasps: stable contact area, finger pose variations and object rotation within/outside stable grasps. Note that hand wrist pose changes drastically w.r.t. the camera, as shown in Fig 3 in the main paper.

ARCTIC Dataset. In Fig. 9 (top), we plot stable contact area, finger pose variations and object rotation errors on 1303 automatically extracted sequences from ARCTIC-Grasps. Among these three metrics, the stable contact area (top-left) shows the sharpest change within/outside stable grasps. We demonstrate that both the finger poses and the object relative orientation do change during the stable grasps, although their changes are bigger outside grasps. Note that

Category	Duration (sec)			#-clips
	avg	std.	max	
bottle	4.25	4.70	29.40	311
bowl	3.59	5.53	43.36	421
can	3.50	4.11	22.76	105
cup	2.79	3.20	19.72	125
glass	2.45	3.73	34.72	226
mug	2.40	3.34	29.74	167
pan	6.39	9.36	91.28	526
plate	2.77	4.49	54.60	473
saucepan	5.73	10.08	76.10	77
All	3.95	6.30	91.28	2431

Table 7: EPIC-Grasps sequences statistics

Category	Duration (sec)			#-clips
	avg	std.	max	
box	1.52	0.75	4.23	138
capsulemachine	1.51	0.69	3.60	95
espressomachine	1.72	0.95	4.73	101
ketchup	1.51	0.80	4.83	106
laptop	1.39	0.74	4.90	144
microwave	1.51	0.81	5.53	112
mixer	1.44	0.68	3.30	122
notebook	1.15	0.44	2.83	151
phone	1.30	0.91	8.07	146
scissors	1.60	0.77	4.37	57
waffleiron	1.21	0.58	3.90	131
All	1.42	0.76	8.07	1303

Table 8: ARCTIC-Grasps sequences statistics

the top-left and top-right plots in Fig. 9 are the same as those in Fig 4 of the main paper.

Furthermore, we manually annotate 40 stable grasps in ARCTIC dataset, by observing the videos solely without using the 3D ground truth. We plot the three metrics in Fig. 9 (bottom). As expected, Fig. 9 (bottom-left) shows that the stable grasp duration corresponds to a consistent in-contact area for manual annotated stable grasps. We also verify that the rotation approximation error of 1-DoF are smaller than Static for manually obtained annotations. These figures confirm that the automatically extracted stable grasps are a good approximation of manual annotations of stable grasps.

HOI4D Dataset. To showcase our assumptions on stable grasp generalise to other datasets with 3D annotations, we replicate the analysis above, on the publicly available HOI4D dataset [28]. We use the Eq (2) again to obtain 3568 stable grasps sequences from the HOI4D. Note that the noise of the 3D ground truth pose in HOI4D are much higher than ARCTIC, we thus increase the contact dis-

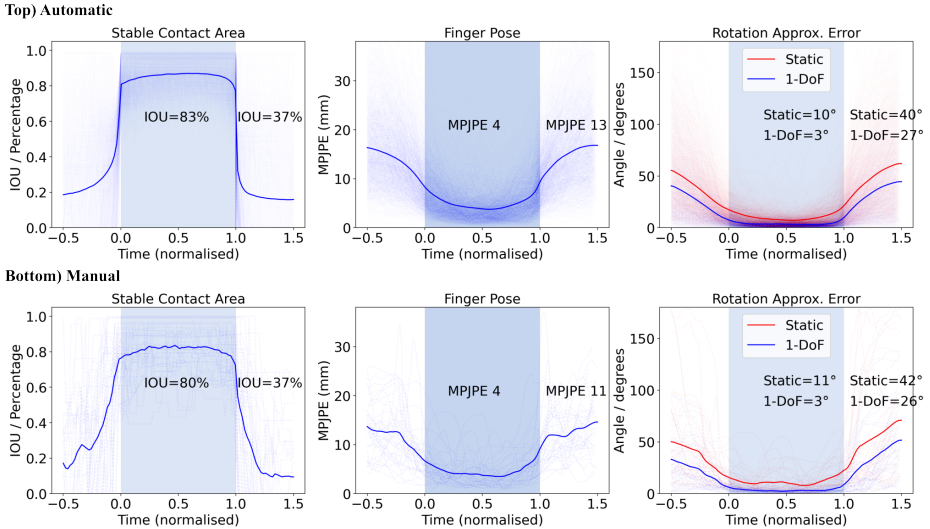


Fig. 9: Metrics on ARCTIC within/outside stable grasps: Comparing object in-contact area (left), finger pose (middle) and relative object rotation w.r.t. the hand. Normalising all stable grasp duration for direct comparison.

distance threshold to 1cm (from 0cm in ARCTIC) and set τ to a lower value 0.3. As in ARCTIC, we also manually annotate 60 stable grasps in HOI4D dataset, by observing the videos, and compute the same metrics.

In Fig. 10, we compare the three metrics on the stable grasp sequences on HOI4D, for both automatic annotations (top) and manually annotated samples (bottom). As expected, the stable contact area shows sharp drops at the temporal boundary of stable grasps. Similarly, we observed that the object do rotate relative to the hand, while the rotation error off the 1-DoF axis are much smaller.

These figures showcase that:

- Our definition of the stable contact temporal duration extends to multiple 3D-annotated datasets.
- On a variety of datasets, subjects and manipulated objects, the finger poses exhibit considerable changes during the stable grasp.
- On both datasets and all sequences, objects rotate within the stable grasp – the static assumption produces a large error within the stable grasp (11° in ARCTIC compared to 12° in HOI4D).
- Optimising for the rotation around a latent axis, the error off the 1-DoF assumption is significantly smaller and better corresponds to the stable grasp temporal extent. This conclusion is verified on both datasets and both manual and automatically annotated sequences.

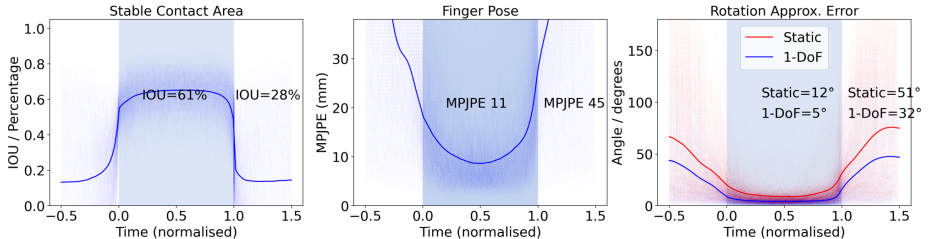
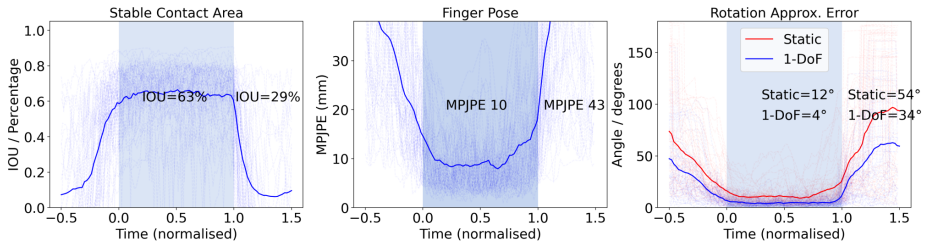
Top) Automatic**Bottom) Manual**

Fig. 10: Metrics on HOI4D within/outside stable grasps: Comparing object in-contact area (left), finger pose (middle) and relative object rotation w.r.t. the hand. Normalising all stable grasp duration for direct comparison.

D Evaluating CAD-agnostic method IHOI

In our method, we assume knowledge of the CAD model. We also explored the recent works that attempt hand grasps without such knowledge. In this section, we showcase these models to be unusable for in-the-wild stable grasp reconstruction through three examples, qualitatively.

The shape reconstruction method proposed in [21] requires careful scan of the underlying in-hand object hence is not suitable for testing in our case. We also note that HOLDNet [12] and DiffHOI [48] do not have released code to be used. Therefore, we evaluate the image-based CAD-agnostic method IHOI [47] on the EPIC-Grasps dataset, using a model trained on HO3D [17] images that contain the same categories: mug and bottle – i.e. the method is aware of these shapes during training.

Fig. 11 shows IHOI is unable to generate plausible object meshes. As fingers are mostly occluded in egocentric views, this makes the challenge of reconstruction significantly higher than side-view reconstructions where fingers are mostly visible. While CAD-agnostic reconstruction is the ultimate goal, these approaches are currently far from being useful for our scenario.

E Ablation on hand pose estimation method

While we use the recent transformer-based approach for estimating hand-pose, HaMeR [32], we test our method using the FrankMocap baseline for hand pose estimation [35]. This is an important ablation as our baseline uses FrankMocap.



Fig. 11: In-the-wild test of IHOI [47]

In Tab. 9, we showcase that our method, using FrankMocap [35] for hand pose estimation outperforms the baseline HOMan [18] which also uses FrankMocap. Using the same hand initialisation, we outperform HOMan [18] by a wide margin - SCA@0.6 improves from 3.3 to 20.3. Using HaMeR, the method further improves consistently over all categories. Average SCA@0.6 improves by an additional 12.6% to reach 32.9.

Fig. 12 shows that FrankMocap struggles with the hand orientation, resulting in incorrect reconstruction results.

F Further Implementation Details

Physical Heuristics In Eq (5) of the main paper we note our usage of physical attraction and repulsion losses E_{push} and E_{pull} .

The term E_{push} ensures all object vertices are located inside the contact surface of the hand (Fig 13). For each $v_o \in V_o$, we locate the nearest vertex in hand contact regions, and compute distance along the surface normal of this hand vertex. Object vertices that penetrate into the contact surface will have negative values. We maximise those negative values, truncating the positive ones:

$$E_{push}^n = \sum_{v_o \in V_o} -1 * \min(d_v, 0) \quad (7)$$

$$d_v = \langle v_o - v_h^*, n_h^* \rangle \quad (8)$$

where v_h^* is the corresponding nearest vertex on the hand and n_h^* is the surface normal of v_h^* .

Category	HOMan [18]			1-DoF + FrankMocap			1-DoF + HaMeR		
	IOU	SCA@0.8	SCA@0.6	IOU	SCA@0.8	SCA@0.6	IOU	SCA@0.8	SCA@0.6
bottle	56.7	3.4	5.8	66.7	11.7	36.8	72.1	26.1	51.3
bowl	54.4	1.1	1.6	53.5	5.5	14.4	56.2	11.1	25.7
can	48.3	3.4	5.1	53.1	11.0	20.9	54.1	16.5	26.6
cup	56.9	5.5	7.8	64.2	11.5	32.5	65.9	18.4	46.1
glass	55.4	3.0	4.2	58.8	10.7	25.7	62.5	15.7	37.8
mug	59.4	3.9	6.6	61.1	7.0	28.3	62.6	10.8	38.6
pan	48.3	0.5	1.9	39.7	2.0	6.9	49.1	7.0	20.4
plate	61.1	1.0	1.6	61.0	9.0	21.5	65.2	16.3	34.6
saucepans	51.1	0.4	2.4	51.4	1.8	16.2	56.8	8.5	34.6
All	54.9	1.9	3.3	55.1	7.2	20.3	59.9	14.1	32.9

Table 9: Ablation on the hand pose estimation method. Green shows the best per metric, Yellow shows the second best.

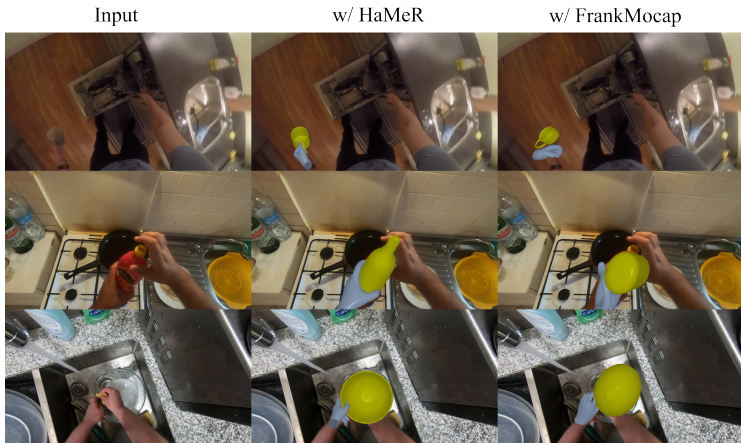


Fig. 12: Qualitative comparison between HaMeR and FrankMocap, when used with our method.

In addition to E_{push} , which pushes the object out of the penetrating region against the hand, we use a balancing loss E_{pull} which pulls the object to touch these contact regions. We here focus on the eight contact regions showcased in Fig 13. For each contact region with hand vertices $\{v_h\}_C$, the region-to-object distance is defined as the minimum distance of all (v_h, v_o) pairs. We use 5 finger tip regions and minimise the average of these region-to-object distances.

$$E_{pull}^n = \frac{1}{5} \sum_C d(\{v_h\}_C, V_o) \quad (9)$$

$$d(\{v_h\}_C, V_o) = \min_{v_h \in \{v_h\}_C, v_o \in V_o} \langle v_h - v_o, n_o \rangle \quad (10)$$

where n_o is the surface normal of v_o .



Fig. 13: Eight contact regions: five finger tips + three palm areas. The contact regions serve two purposes: bounding the object inside and attracting the object closer to these regions.

Initialisation of poses on EPIC-Grasps. For EPIC-Grasps dataset, we manually set initial object relative poses to the common poses of each category, results in 80 total initial poses for 9 object categories.

Initialisation of poses on ARCTIC-Grasps. For ARCTIC-Stable dataset, the initial rotations are generated by clustering the ground-truth rotations, where clustering is performed via the axis-angle representation of the rotation matrix. We initialise 50 rotations and 1 global translation for each (object, left/right hand) pair.